Molecular Therapy
Oncolytics
Original Article

Hsa_circ_0001666 promotes non-small cell lung cancer migration and invasion through miR-1184/miR-548I/AGO1 axis

Xueting Wang,[1] Rui Li,[3] Lingxin Feng,[1] Jing Wang,[1] Qi Qi,[1] Wenjie Wei,[2] and Zhuang Yu[1]

[1]Department of Oncology, The Affiliated Hospital of Qingdao University, Qingdao University, Qingdao 266000, China; [2]Department of Urology, Union Hospital, Tongji Medical College, Huazhong University of Science and Technology, Wuhan 430022, China; [3]Health Management Center, The Affiliated Hospital of Qingdao University, Qingdao University, Qingdao 266000, China

Accumulating evidence has revealed that the dysregulation of circular RNAs (circRNAs) plays crucial roles in the occurrence and progression of cancers. However, the aberrant expression profile and dysfunction of circRNAs in non-small cell lung cancer (NSCLC) have not been fully explored. Herein, we discovered that a circRNA, hsa_circ_0001666 (circ0001666), was highly expressed in NSCLC tissues and cell lines, and it was positively correlated with NSCLC tumor pathological grade and lymph node metastasis. Moreover, Kaplan-Meier survival analysis implied that NSCLC patients with high circ0001666 expression were negatively correlated with favorable survival. Functionally, circ0001666 could promote migration and invasion of NSCLC cells *in vitro* and *in vivo*. Mechanistically, circ0001666 could act as a sponge to miR-1184/miR-548I and upregulate the expression of AGO1, thereby promoting the activation of the phosphatidylinositol 3-kinase (PI3K)/AKT/mTOR signaling pathway in NSCLC cells. Collectively, these findings demonstrated that circ0001666 could serve as an oncogene to promote the migration and invasion of NSCLC via a novel miR-1184/miR-548I/AGO1 axis, which might be a promising therapeutic target for NSCLC treatment.

INTRODUCTION

Nowadays, lung cancer is the most common cause of cancer deaths worldwide, accounting for almost a quarter of all cancer deaths. In 2021, more than 100,000 Americans will die of lung cancer.[1] Approximately 85% of lung cancer patients have a group of histologic subtypes collectively known as non-small cell lung cancer (NSCLC), including lung adenocarcinoma (LUAD), lung squamous cell carcinoma (LUSC), and large cell carcinoma.[2,3] At present, for the standardized treatment of NSCLC, surgical resection and chemotherapy have demonstrated their favorable effect on earlier stage disease, and the combination of chemotherapy and radiotherapy has been considered the recommended therapy for patients with unresectable locally advanced NSCLC.[2] Furthermore, targeted therapy and immune checkpoint blockers (ICBs) have also been shown tremendous benefits for advanced NSCLC patients.[4–6] Although there have been chemotherapy, targeted therapy, and immunotherapy developed and commonly applied in clinical NSCLC treatment,[2] the overall survival rate of NSCLC remains low due to the high rate of distant metastasis, regional recurrence, and innate or acquired drug resistance.[7–9] As NSCLC is highly heterogeneous and intricate in molecular pathogenesis,[10] the molecular mechanisms underlying the development and progression of NSCLC still need to be further elaborated in detail. Therefore, it is urgent to illuminate the pathogenesis of NSCLC and seek a new therapeutic approach, thereby improving survival outcomes in patients with NSCLC.

Circular RNAs (circRNAs), which derive from pre-mRNA back splicing, are a type of non-coding RNA characterized by covalently closed loop structures without 5′ terminal caps or a 3′ terminal poly (A) tail.[11,12] The unique close structure of circRNAs renders a stronger resistance to exonucleases and consequently improves its stability, and they have been considered as clinical non-invasive diagnostic markers in cancer.[13–17] With the rapid development of RNA sequencing technology and bioinformatics, more than 100,000 circRNAs have been identified in cells.[18] Among them, some circRNAs have been implicated to be involved in diverse biological processes of NSCLC. For example, circNDUFB2 could inhibit the growth and metastasis of NSCLC via destabilizing IGF2BPs and activating antitumor immunity.[19] CircFGFR1 could directly sponge to miR-381-3p and subsequently upregulate the expression of the CXCR4, which promoted NSCLC progression.[20] CircPTK2 could inhibit transforming growth factor β (TGF-β)-induced epithelial-mesenchymal transition and metastasis by upregulating TIF1γ in NSCLC.[21] Noteworthily, several studies have shown that circ0001666 plays a carcinogenic role in papillary thyroid carcinoma and pancreatic cancer.[22,23] However, the function of circ0001666 involved in NSCLC is unclear.

Received 29 September 2021; accepted 11 February 2022;
https://doi.org/10.1016/j.omto.2022.02.011.

Correspondence: Wenjie Wei, Department of Urology, Union Hospital, Tongji Medical College, Huazhong University of Science and Technology, Wuhan 430022, China.
E-mail: wenjieweidoc@outlook.com
Correspondence: Zhuang Yu, Department of Oncology, The Affiliated Hospital of Qingdao University, Qingdao University, Qingdao 266000, China.
E-mail: yuzhuang2002@163.com

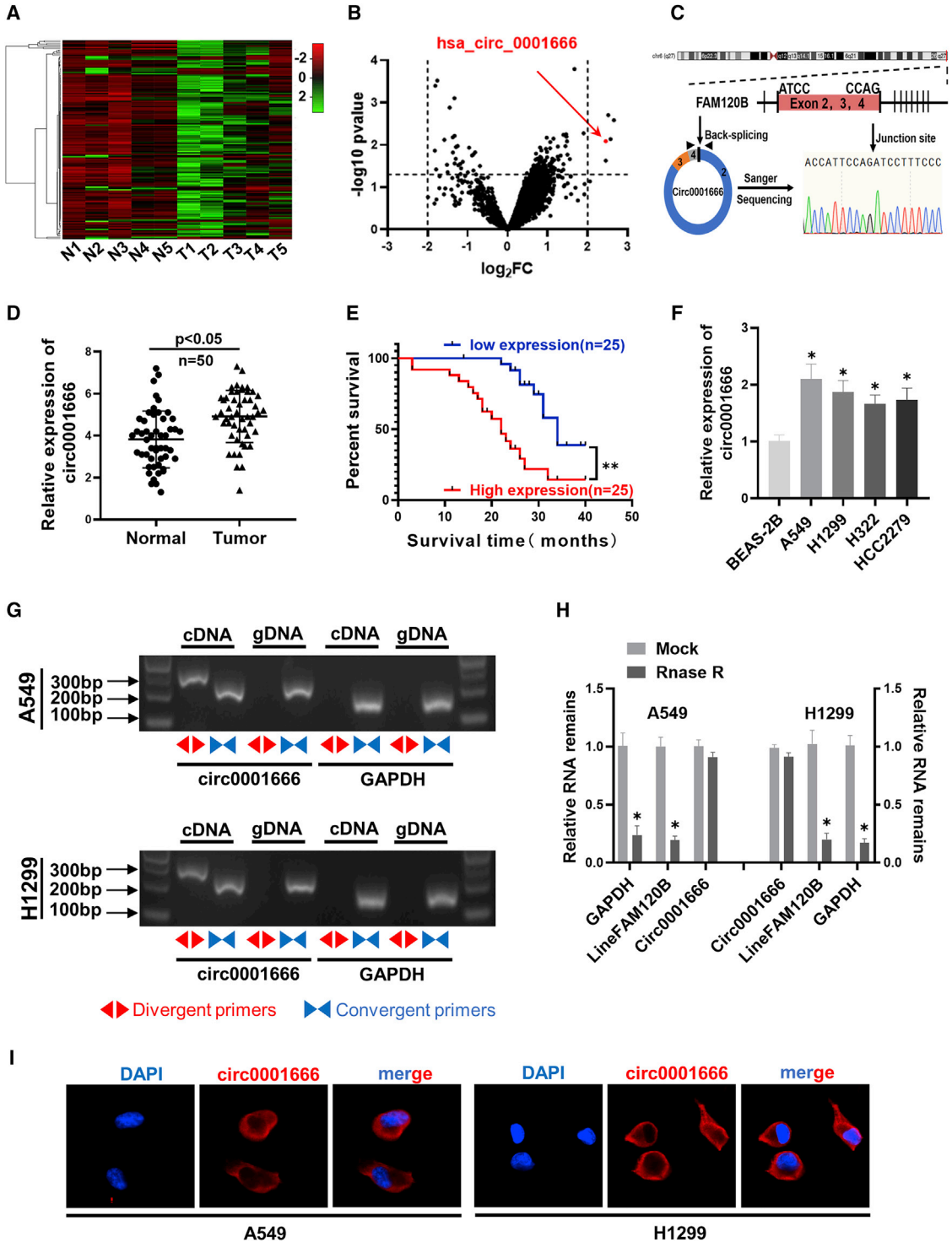

Figure 1. The validation and characteristics of circ0001666 in NSCLC

(A and B) GEO database (GEO: GSE101586) depicted the identification of circ0001666 in NSCLC. (C) Schematic illustration of circ0001666 formation and the results of Sanger sequencing is shown. (D) The expression levels of circ0001666 in 50 pairs of NSCLC and corresponding adjacent tissues were detected by quantitative real-time PCR. (E) Kaplan-Meier's analysis of correlation between circ0001666 expression level and overall survival of 50 patients with NSCLC (log rank test) is shown. (F) The expression levels of circ0001666 were detected by quantitative real-time PCR in normal human bronchial epithelial cells (BEAS-2B) and NSCLC cell lines (A549, H1299,

(legend continued on next page)

Further insight into the roles and mechanisms of circ0001666 in NSCLC may expand and update circRNAs involved in lung cancer.

MicroRNAs (miRNAs), as another member of the non-coding RNA family that function as post-transcriptional regulators of target mRNAs, have been discovered to possess great potential for affecting proliferation, migration, angiogenesis, apoptosis, autophagy, and drug resistance in NSCLC.[24–26] For example, miRNA-124 could bind to the 3′ UTR of SOX9 to upregulate the expression of SOX9, thereby repressing the proliferation and metastasis of NSCLC.[27] miRNA-338-3p could bind to the 3′ UTR of SphK2 to induce apoptosis in lung cancer.[28] However, the upstream regulators of miRNAs are yet to be clarified in detail. Interestingly, researchers have shown that some circRNAs contain miRNA response elements (MREs) and interact with miRNAs as "miRNA sponges" to make a negative regulation on miRNAs.[12] One extreme case is CDR1as, which contains over 70 binding sites of miR-7 and intensely inhibits the miR-7 activity, resulting in increased levels of miR-7 targets.[29] However, the function of circRNAs as miRNA sponges has not been clearly elucidated in NSCLC yet.

In view of understanding circRNAs-mediated oncogenic development of NSCLC, we focused on the upregulated circRNAs based on existing published RNA sequencing data of human NSCLC and normal lung tissues. We further demonstrated that circ0001666, which originated from exons 2, 3, and 4 of the FAM120B gene, was significantly upregulated in NSCLC tissues and cell lines. Functional and mechanistic investigations revealed that circ0001666 could act as a sponge for miR-1184 and miR-548I to relieve miRNAs repression of target gene AGO1, which activated the phosphatidylinositol 3-kinase (PI3K)/AKT/mTOR signaling pathway, promoting migration and invasion of NSCLC. Taken together, these findings unveil the clinical impact, biological roles, and underlying mechanisms of circ0001666, and it might serve as a novel potential therapeutic target for NSCLC.

RESULTS

Circ0001666 is highly expressed in NSCLC tissues and cell lines and is predominantly localized in the cell cytoplasm

To characterize dysregulated circRNAs in NSCLC, we analyzed the GEO database (GEO: GSE101586) of five human NSCLC tissues and paired adjacent non-tumor tissues and found that circ0001666, which is named hsa_circ_0001666 in circBase (http://www.circbase.org), was notably upregulated in NSCLC tissues (Figures 1A and 1B). The genomic structure indicates that circ0001666 is generated from the three exons (exons 2, 3, and 4) of pre-FAM120B mRNA in a "back-splicing" way, and the existence of circ0001666 was confirmed with Sanger sequencing (Figure 1C). Then, we measured the expression level of circ0001666 in 50 cases of NSCLC tissues and their corresponding paracancerous tissues. A more significant upregulation of circ0001666 expression was observed in NSCLC tissues compared with their adjacent non-tumorous tissues (Figure 1D). Intriguing, high expression of circ0001666 was positively associated with lymph node metastasis and pathological stage in NSCLC patients (Table 1). In addition, Kaplan-Meier survival analysis implied that NSCLC patients with high circ0001666 expression level had a poor survival time (Figure 1E). Moreover, the expression level of circ0001666 was significantly upregulated in A549, H1299, H322, and HCC2279 cells, in comparison with the normal bronchial epithelial cell line (BEAS-2E; Figure 1F).

Table 1. Clinicopathological features and expression of circ0001666 in 50 patients with NSCLC

Clinicopathological features	Group	Number of patients	circ0001666 expression		p value
			Low	High	
Age	<60	13	8	5	
	≥60	37	17	20	0.5202
Gender	male	29	13	16	
	female	21	12	9	0.5672
Smoker	smoker	18	6	12	
	nonsmoker	32	19	13	0.1398
Tumor size (cm)	<3	19	14	5	
	≥3	31	11	20	0.0186
Lymph node metastasis	no	20	16	4	
	yes	30	9	21	0.0012
Stage	I+II	22	15	7	
	III+IV	28	10	18	0.0450
Total		50	25	25	

Chi-square (or Fisher's exact) test.

To rule out the possibilities of *trans*-splicing or genomic rearrangements, two steps were taken to prove the existence of circ0001666 head-to-tail splicing. First, we designed convergent primers and divergent primers to amplify linear FAM120B mRNA and circ0001666 based on cDNA and genomic DNA (gDNA) extracted from A549 and H1299 cell lines. As shown in Figure 1G, circ0001666 could only be amplified with divergent primers in cDNA, but not in gDNA. Secondly, we pretreated the total RNA with RNase R and identified that the expression of circ0001666 was enriched, whereas the expression of linear FAM120B was significantly reduced after RNase R treatment (Figure 1H), which suggested circ0001666 was more stable than linear FAM120B. Then, we performed RNA fluorescence *in situ* hybridization (FISH) assays to identify the subcellular localization of circ0001666. The images indicated that circ0001666 was mainly localized in the cytoplasm (Figure 1I).

H322, and HCC2279). (G) The existence of circ0001666 was verified by gel electrophoresis with convergent or divergent primers in A549 and H1299 cell lines. (H) The expression levels of circ0001666 and FAM120B mRNA after treatment with or without RNase R were measured by quantitative real-time PCR in A549 and H1299 cells. (I) FISH images showed the subcellular localization of circ0001666 in A549 and H1299 cells. circ0001666 was stained red with Cy3, and the nuclei was stained blue by DAPI. Data are presented as the means ± SEM of three independent experiments. *$p < 0.05$.

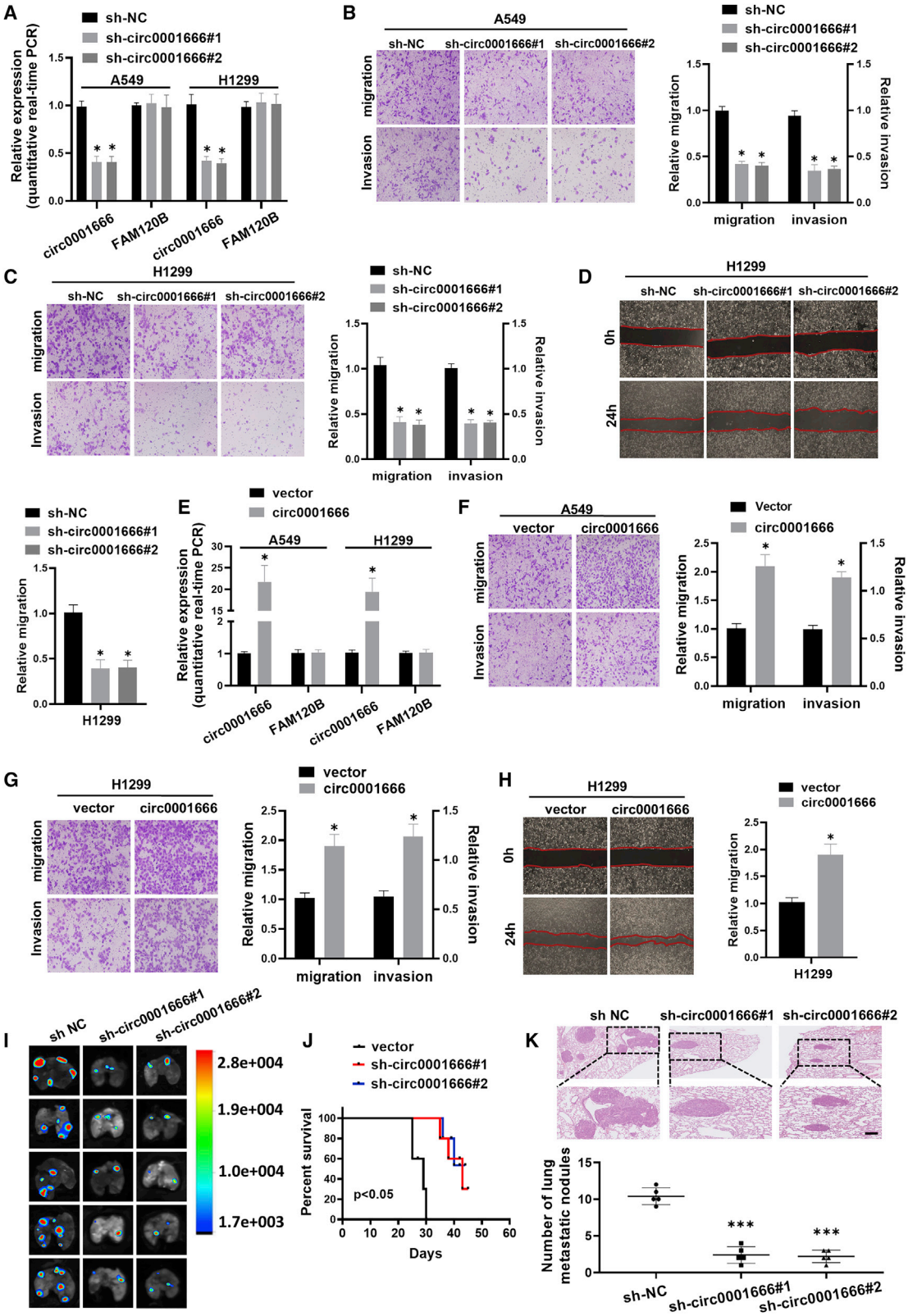

(legend on next page)

Taken together, these data indicated that circ0001666 was upregulated in NSCLC and predominantly localized in the cell cytoplasm.

Circ0001666 promotes migration and invasion of NSCLC cells

To investigate the potential biological effect of circ0001666 on NSCLC cells, we established stable models of circ0001666 overexpression or knockdown in A549 and H1299 cell lines, respectively. The overexpression and knockdown efficiencies of circ0001666 were detected by quantitative real-time PCR (Figures 2A and 2E). Knockdown of circ0001666 suppressed cell migration and invasion abilities in both A549 and H1299 cells (Figures 2B and 2C), while overexpression of circ0001666 promoted NSCLC cells migration and invasion (Figures 2F and 2G). Simultaneously, wound healing assays showed similar results (Figures 2D and 2H). In addition, we established a nude mouse lung metastasis model by tail vein injecting of circ0001666-knockdown A549 cells. Bioluminescence imaging showed circ0001666-knockdown mice had decreased the number of pulmonary metastasis foci (Figure 2I). Moreover, mice with low circ0001666 expression level had a favorable overall survival (Figure 2J). Meanwhile, H&E staining confirmed that mice with circ0001666 knockdown exhibited significantly fewer and smaller metastatic tumor nodules in the lungs (Figure 2K). Taken together, these experiments demonstrated that circ0001666 could promote the migration and invasion of NSCLC cells in both *in vitro* cell culture and *in vivo* mouse models, although the tail-vein injection of tumor cells is not a spontaneous metastasis model.

Circ0001666 directly binds to miR-1184 and miR-548I in NSCLC cells

Previous studies have shown that circRNAs located in the cytoplasm might serve as a miRNA "sponge."[30] To determine whether circ0001666 localized in cytoplasm acted as a miRNA sponge, we performed anti-Argonaute2 (anti-AGO2) reciprocal immunoprecipitation (RIP) assay and found that circ0001666 was significantly enriched by AGO2 antibody compared with immunoglobulin G (IgG) in A549 and H1299 cells (Figure 3A). Those results implied that circ0001666 might function as a miRNA sponge in NSCLC. Then, we designed the biotinylated circ0001666 probe and performed RNA pull-down assays. The efficiency and specificity of the circ0001666 probe were verified by quantitative real-time PCR and gel electrophoresis. The results showed that circ0001666 could be specifically enriched by the circ0001666 probe in NSCLC cells (Figures 3B and 3C). In Figure 3D, 10 miRNAs were predicted to be potential targets of circ0001666 through determining the overlap of predictions from three bioinformatics databases (CircInteractome, miRanda, and Circbank). Subsequently, we conducted pull-down assays with the biotinylated circ0001666 probe and performed quantitative real-time PCR analysis on 10 candidate miRNAs. Among 10 candidate miRNAs, miR-1184 and miR-548I could be abundantly pulled down by the circ0001666 probe in both A549 and H1299 cells (Figures 3E and S1A). To further confirm the sponge effect between circ0001666 and miR-1184/miR-548I, we constructed circ0001666 wild-type and mutant dual luciferase reporter vectors (Figure 3F). Upregulation of miR-1184 and miR-548I could significantly decrease relative luciferase activity of the wild-type circ0001666 reporter vector, but not the mutant reporter vector, in NSCLC cells (Figures 3G and S1B). We also applied biotin-labeled miR-1184 and miR-548I wild-type or mutant mimics to verify the direct binding of circ0001666 and miRNAs in NSCLC cells. The results all showed that biotin-labeled miR-1184/miR-548I wild-type mimics captured more circ0001666 than the mutant mimics in NSCLC cell lines (Figures 3H, 3I, S1C, and S1D). Moreover, FISH assays showed that circ0001666 was co-localized with miR-1184/miR-548I in the cytoplasm (Figure 3J). The above results suggested that circ0001666 could directly bind to miR-1184 and miR-548I in NSCLC cells.

miR-1184 and miR-548I inhibit NSCLC cells migration and invasion and weaken the oncogene role of circ0001666

Next, we further evaluated the potential functional roles of miR-1184 and miR-548I in NSCLC. We transfected miRNA mimics or miRNA inhibitors into A549 and H1299 cells to conduct transwell assays and wound healing assays. Compared with the mimic NC group, the migration and invasion abilities of A549 and H1299 cells transfected with miR-1184/miR-548I mimics were significantly inhibited. In contrast, the transfection with miR-1184/miR-548I inhibitors had the opposite effect (Figures 4A and 4B). Subsequently, rescue experiments confirmed that circ0001666 could reverse the inhibition of cell migration and invasion induced by miR-1184/miR-548I in A549 and H1299 cells (Figures 4C and 4D). Collectively, these results demonstrated that circ0001666 facilitated NSCLC cells migration and invasion partly through impairing the tumor-suppressor role of miR-1184 and miR-548I.

Circ0001666 positively regulates AGO1 expression by interacting with miR-1184/miR-548I in NSCLC cells

Given that we identified the function link between circ0001666 and miR-1184/548I, we next aimed to explore downstream molecules regulated by the circ0001666/miR-1184/548I axis. We first used miRDB and

Figure 2. circ0001666 promotes invasion and metastasis of NSCLC cells *in vitro* and *in vivo*

(A) The expression levels of circ0001666 and FAM120B mRNA in A549 and H1299 cells after stable transfection with sh-circ0001666 or sh-NC were detected by quantitative real-time PCR. (B and C) Cell migration and invasion capabilities were assessed by transwell assays after knocking down circ0001666 in A549 (B) and H1299 (C) cells. (D) Cell migration capabilities were evaluated by wound healing assays after knocking down circ0001666 in H1299 cells. (E) The expression levels of circ0001666 and FAM120B mRNA in A549 and H1299 cells after stable transfection with circ0001666 or vector were detected by quantitative real-time PCR. (F and G) Cell migration and invasion abilities of A549 (F) and H1299 (G) cells transfected with circ0001666 or vector were assessed by transwell assays. (H) Cell migration abilities were evaluated by wound healing assays after transfecting with circ0001666 or vector in H1299 cells. (I) Fluorescence images showed metastatic intrapulmonary lesions colonized in nude mice after stable transfection with circ0001666 knockdown or control lentiviral vectors. (J) Kaplan-Meier curves analysis showed the effect of knockdown circ0001666 on the survival of nude mice. (K) Hematoxylin and eosin (H&E) staining was performed for histological confirmation of metastasizing tumor cells in lung. Bar graphs show the statistical analysis of three independent experiments. $^{*}p < 0.05$, $^{***}p < 0.001$.

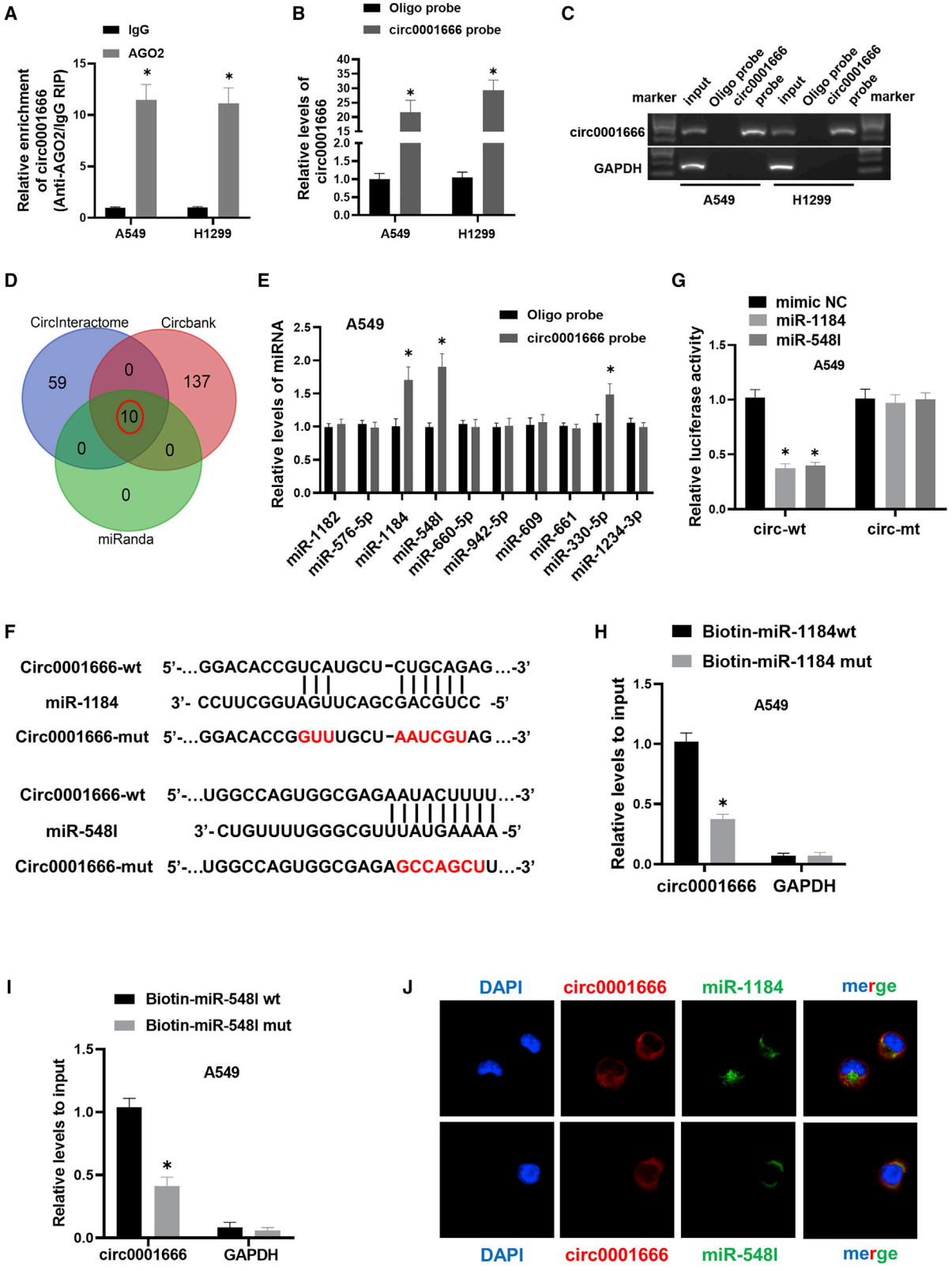

(legend on next page)

TargetScan to search for possible target genes that miR-1184/miR-548I could bind to in NSCLC and found 44 potential target genes. Previous evidence has shown that circRNAs could act as a miRNA sponge to terminate the interaction between miRNA and the 3′ untranslated region (3′ UTR) of its target mRNA, alleviating mRNA degradation or post-translational inhibition of gene expression.[31] Based on these findings, we screened for targeted genes that were highly expressed in NSCLC in the The Cancer Genome Atlas (TCGA) database and found a total of 17 overlapped potential target genes. Subsequently, we explored the correlation between circ0001666 and 17 target genes and verified that six target genes were positively correlated with circ0001666 (Figure S2). Among six candidate genes, AGO1 had the most significant positive correlation with circ0001666 (Figure 5A). Furthermore, the quantitative real-time PCR assay indicated that overexpression of circ0001666 could enhance the expression of AGO1 in A549 and H1299 cells (Figure 5B). Thus, we speculated that circ0001666 might perform its function via AGO1 in NSCLC. Next, luciferase reporters containing wild-type and mutated putative binding sites of AGO1 3′ UTR transcript were constructed. Dual-luciferase reporter assays showed that miR-1184/miR-548I inhibitors could significantly improve the wild type of AGO1 3′ UTR luciferase reporter activity, but there was no obvious effect on the mutant of AGO1 3′ UTR luciferase reporter activity (Figure 5C). Consistently, western blot analysis indicated that the expression of AGO1 protein was significantly decreased after transfecting miR-1184/miR-548I mimics, whereas AGO1 protein level was upregulated after transfection with miR-1184/miR-548I inhibitors in A549 and H1299 cells (Figure 5D). These results suggested that miR-1184/miR-548I could be able to bind to AGO1 mRNA 3′ UTR and inhibit its expression (Figure 5D). Furthermore, rescue experiments were performed in NSCLC cells and demonstrated that circ0001666 reversed the reduction of AGO1 mRNA level induced by miR-1184/miR-548I (Figure 5E). In addition, western blotting assays displayed that circ0001666 could reverse the reduction of AGO1 protein expression induced by miR-1184/miR-548I in NSCLC cells (Figure 5F). Therefore, circ0001666 could directly bind to miR-1184/miR-548I in NSCLC cells, thereby promoting the expression of the downstream target AGO1.

AGO1 is upregulated in NSCLC cells and promotes NSCLC cell migration and invasion

Subsequently, we measured the expression of AGO1 in 50 pairs of NSCLC tissues and matched adjacent normal tissues using quantitative real-time PCR. The result showed that AGO1 was upregulated in NSCLC tissues (Figure 6A). Next, we established cell lines with stable knockdown of AGO1 and overexpression of AGO1. The efficiencies of AGO1 knockdown and overexpression were analyzed by quantitative real-time PCR and western blotting (Figure 6B). As shown in Figures 6C and 6D, transwell assays and wound healing assays illustrated that overexpression of AGO1 resulted in remarkably increased migration and invasion of NSCLC cells, while knockdown of AGO1 significantly suppressed these phenotypes. Knockdown of circ0001666 could reverse the promotion of migration and invasion abilities induced by ectopic expression of AGO1 (Figures 6E and 6F). Collectively, these results indicated that AGO1 promoted NSCLC migration and invasion, which was partially mediated by circ0001666.

Circ0001666 activates the PI3K/AKT/mTOR signaling pathway by enhancing the expression of AGO1

In addition, we explored the potential signaling pathway involved in circ0001666. Based on the NSCLC mRNA expression data of the TCGA, gene set enrichment analysis (GSEA) was performed. We found that high expression of AGO1 was positively correlated with the activation of PI3K/AKT/mTOR signaling pathway (Figures 7A–7C), which was a well-known cancer-promoting pathway in NSCLC.[32] We then examined whether circ0001666 could affect the PI3K/AKT/mTOR signaling pathway. As shown in Figure 7D, overexpression of circ0001666 significantly increased the expression of phospho-PI3K/AKT/mTOR proteins, which suggested circ0001666 might promote the activation of PI3K/AKT/mTOR signaling pathway. Meanwhile, the upregulated expression of these proteins induced by circ0001666 could be significantly reduced by silencing of AGO1 (Figure 7D). Collectively, the above results illuminated that circ0001666 could activate PI3K/AKT/mTOR signaling pathway through facilitating the expression of AGO1 in NSCLC.

DISCUSSION

Despite significant advances in diagnosis and treatment of lung cancer, it remains the most frequent cause of cancer-related mortality worldwide. Underlying mechanisms of occurrence and development in NSCLC remain to be further clarified. Therefore, exploring a novel molecular target is urgently needed. In the past few years, an increasing number of circRNAs have been reported as important drivers of tumor formation or tumor suppressors in human cancers.[33] Meanwhile, circRNAs are expressed more stably and specifically in cells, tissues, and body fluids than other RNAs, which suggests circRNAs have robust potential to act as the effective biomarker.[31] In our study, we first demonstrated that circ0001666 was frequently upregulated in NSCLC tissues and cells. Functionally, circ0001666 could promote the

Figure 3. circ0001666 could directly bind to miR-1184 and miR-548I in NSCLC cells

(A) Immunoprecipitation (RIP) assay was carried out using anti-AGO2 or IgG antibodies. circ0001666 levels in the samples were quantified using quantitative real-time PCR. (B and C) The efficiency of circ0001666 probe was measured by quantitative real-time PCR and gel electrophoresis. Relative level of circ0001666 was normalized to input. GAPDH was used as negative control. (D) Schematic illustration showed the overlapping target miRNAs of circ0001666 predicted by CircInteractome, miRanda, and Circbank. (E) The relative levels of 10 miRNAs were pulled down by circ0001666 probe or oligo probe in A549 cells. (F) Schematic graph showed the predicted binding sites between circ0001666 and miR-1184/miR-548I and mutation of potential miRNAs binding sequence in circ0001666. (G) The luciferase activities were detected in A549 cells after co-transfection with circ0001666-wt or circ0001666-mut and miR-1184/miR-548I mimics or mimics NC. (H and I) Relative expression levels of circ0001666 were captured by biotinylated wild-type miR-1184/miR-548I or mutant miR-1184/miR-548I. (J) FISH images showed the subcellular co-localization of circ0001666 and miR-1184/miR-548I. circ0001666 was stained red with Cy3, miR-1184/miR-548I were stained green with Dig, and the nuclei were stained blue by DAPI. *$p < 0.05$.

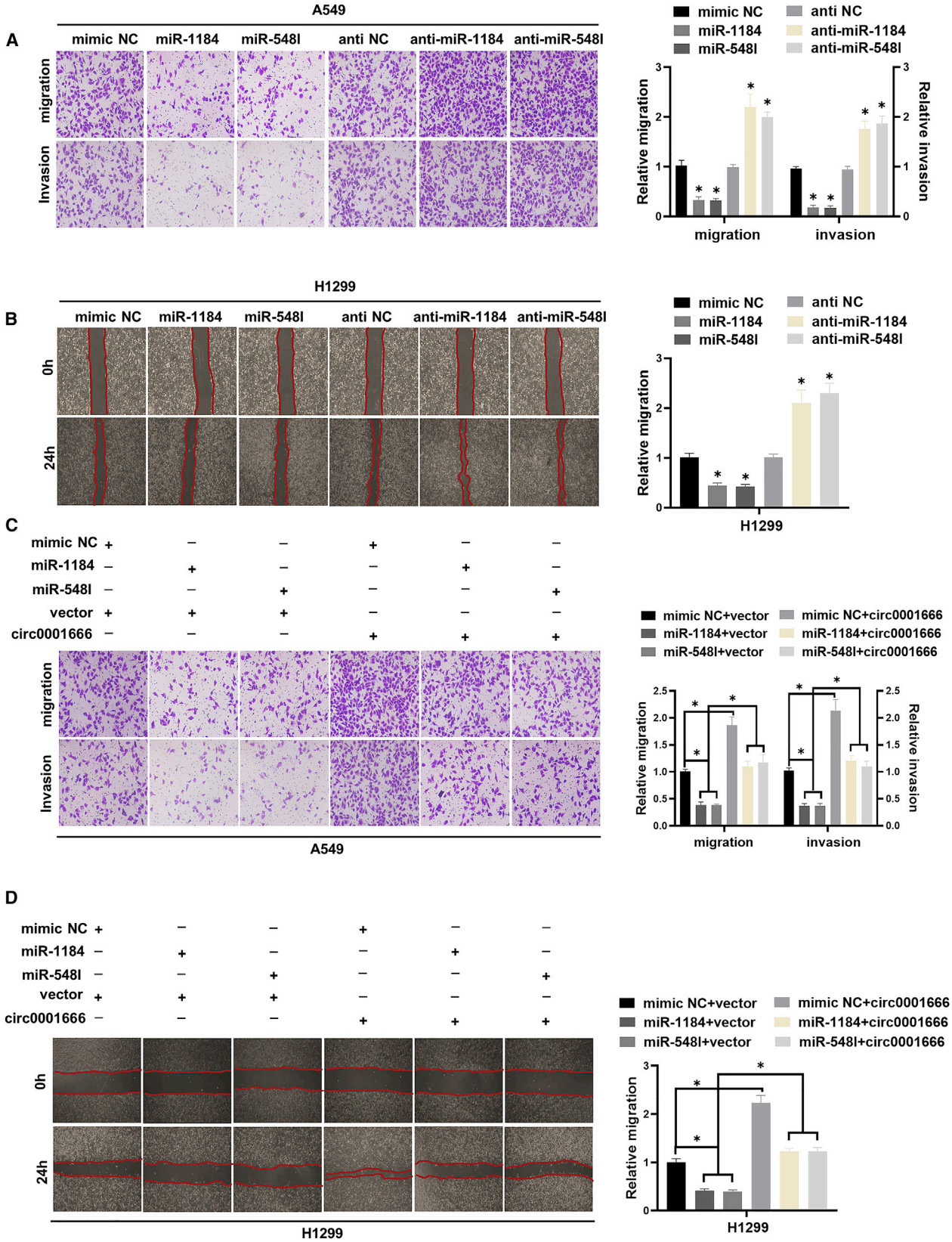

(legend on next page)

migration and invasion of NSCLC cells *in vitro*. Silencing of circ0001666 significantly decreased the number of pulmonary metastasis foci *in vivo*. Taken together, circ0001666 might potentially be used for diagnosis and prognosis evaluation of NSCLC. However, considering that the lung is only the site for origin instead of a metastatic site for NSCLC, the major metastatic sites of NSCLC, such as brain, bone, liver, and thoracic cavity should be further studied. We also notice that the level of steady-state circRNAs expression in cells can be regulated both co- and post-transcriptionally. For example, regulation of circRNAs formation initiates from and is coupled with the transcription of its parental pre-mRNA by RNA polymerase II (RNA Pol II).[34] RNA binding proteins, such as QKI and FUS,[18] can facilitate circRNAs production by binding to and then probably stabilizing back-splicing. Nevertheless, the potential mechanisms leading to the upregulation of circ0001666 in NSCLC remain to be elucidated.

Accumulating studies have demonstrated circRNAs act as the sponge to miRNAs or function by interacting with proteins.[34–36] For example, circACVR2A could directly interact with miR-626 and act as a miRNA sponge to suppress proliferation and metastasis of bladder cancer.[37] Circ-DONSON could facilitate the transcription of SCX4 via recruiting nucleosome remodelling factor (NURF) complex to its promoter, thereby enhancing the proliferation, migration, and invasion of gastric cancer.[38] Hsa_circ_0008367 could physically interact with RNA-binding protein ALKBH5 and positively regulate sorafenib-induced ferroptosis in hepatocellular carcinoma (HCC) cells.[39] In our study, circ0001666 was mainly located in the cytoplasm and could be recognized by AGO2 protein, suggesting that circ0001666 might exert its functions via the classical method of sponging to miRNAs. Subsequently, our study verified that circ0001666 could promote the invasion and migration of NSCLC through binding with miR-1184 and miR-548I simultaneously. Similarly, recent studies also showed that circRNAs could sponge two miRNAs and affect the biological behavior of tumors, such as circ-DICER1,[40] circCRIM1,[41] and circ_0008532.[42] Besides, subsistent data revealed that miR-1184/miR-548I participated in regulating the pathogenesis of various cancers. For instance, miR-1184 inhibited tumor cells growth, migration, and invasion in bladder cancer and colorectal cancer.[43,44] miR-548I could inhibit cells proliferation in HCC.[45] Intriguingly, our study found that miR-1184/miR-548I could inhibit the invasion and migration in NSCLC cells. Subsequent "rescue" experiments confirmed that circ0001666 could reverse the tumor-suppressor roles of miR-1184/miR-548I. Those results confirmed that circ0001666 could regulate the progression of NSCLC by sponging miR-1184/miR-548I.

AGO1, also known as eukaryotic initiation factor 2C1, is a member of the AGO protein family (AGO1–4).[46] Among the AGO protein family, AGO1 has been reported to play an important role in solid tumors. For example, AGO1 could enhance the proliferation and invasion of cholangiocarcinoma by affecting epithelial-mesenchymal transition (EMT)-related TGF-β-PI3K-AKT signaling pathways.[47] AGO1 could promote the growth and metastasis of HCC through activating TGF-β-pathway-associated proteins.[48] Meanwhile, Kim et al.[49] have found that AGO1 may be a novel early diagnostic marker because it is involved in the development of lung cancer. Herein, our data disclosed that miR-1184/miR-548I could directly target the 3′ UTR of AGO1. Down expression of miR-1184 or miR-548I caused the upregulation of AGO1 at mRNA and protein levels. Those results suggested that AGO1 was a downstream target gene of circ0001666/miR-1184/miR-548I regulatory network. Given the oncogenic effect of AGO1 in tumor cells, we focused on whether AGO1 is equally carcinogenic in NSCLC. Significantly, we demonstrated that AGO1 was overexpressed in lung cancer tissues and functionally promoted migration and invasion of NSCLC cells. Meanwhile, our results found circ0001666 upregulated AGO1 at both the mRNA and protein expression levels. Silencing of circ0001666 could partially reverse the increasing of migration and invasion abilities induced by ectopic expression of AGO1. Collectively, circ0001666 could act as an oncogene to promote the invasion and migration through miR-1184/miR-548I/AGO1 axis in NSCLC. In addition, circ0001666 could enhance the activity of PI3K/AKT/mTOR pathway by promoting AGO1 expression. Our findings are supported by the studies of Heavey and colleagues, who showed that genetic activation of PI3K/AKT/mTOR signaling led to tumorigenesis in NSCLC.[32] Collectively, these findings revealed a crucial link between circ0001666 and the PI3K/AKT/mTOR signaling pathway during NSCLC development and progression.

In summary, our current study proved that circ0001666 was overexpressed in NSCLC cell lines and tissues. Functionally, circ0001666 promoted migration and invasion of NSCLC cells both *in vitro* and *in vivo*. Mechanistically, circ0001666 could directly sponge miR-1184 and miR-548I to upregulate AGO1 expression and consequently activate the PI3K/AKT/mTOR signaling pathway. Taken together, our results might prove to be a promising strategy for restraining tumor progression in NSCLC patients.

MATERIALS AND METHODS

Cell culture

Immortalized human bronchial epithelial cells (BEAS-2B) and human lung cancer cell lines (A549, H1299, H322, and HCC2279) were obtained from the Cell Bank of the Chinese Academy of Sciences (Shanghai, China). A549 cells were cultured in F-12 medium (GENOM, China). Other cell lines were cultured in DMED medium (Gibco, USA). All media were supplemented with 10% fetal bovine

Figure 4. miR-1184/miR-548I inhibits NSCLC cell migration and invasion and weakens the oncogene role of circ0001666

(A) Cell migration and invasion abilities of A549 cells transfected with miR-1184/miR-548I mimics or miR-1184/miR-548I inhibitors or negative control were assessed by transwell assays. (B) Cell migration abilities were evaluated by wound healing assays after transfecting with miR-1184/miR-548I mimics or miR-1184/miR-548I inhibitors or negative control. (C) Representative images and quantification results of transwell assays for A549 cells transfected with miR-1184/miR-548I mimics alone or co-transfected with circ0001666. (D) Representative images and quantification results of wound healing assays for H1299 cells transfected with miR-1184/miR-548I mimics alone or co-transfected with circ0001666. *$p < 0.05$.

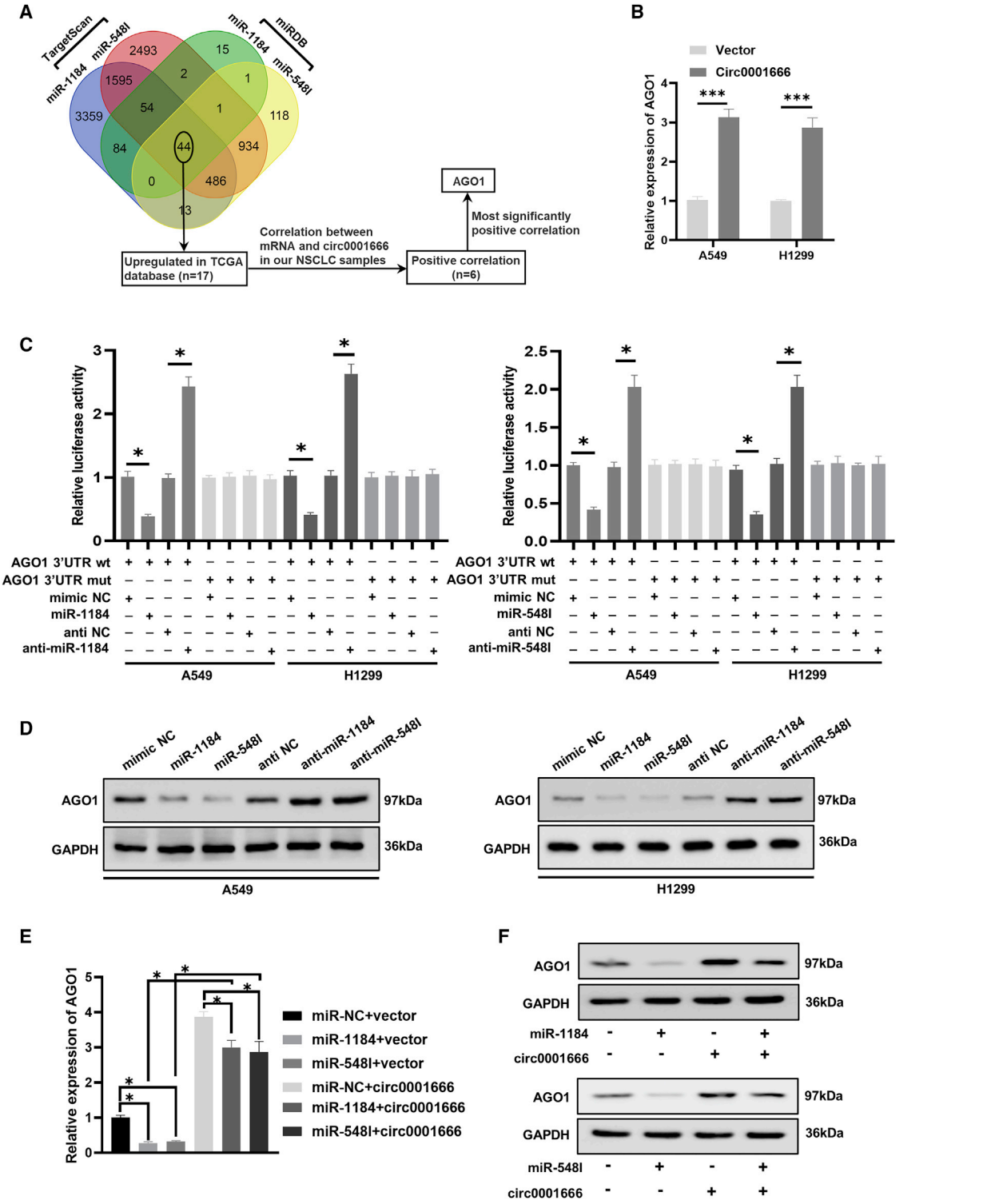

Figure 5. circ0001666 could sponge miR-1184/miR-548I to upregulate AGO1 expression

(A) The Venn diagram showed the possible target genes of miR-1184/miR-548I. (B) The mRNA levels of AGO1 were measured by quantitative real-time PCR in A549 and H1299 cells transferred with circ0001666 overexpression plasmid or control vector. (C) The luciferase activities were detected after co-transfecting with AGO1-3′ UTR-wt or

(legend continued on next page)

serum (Gibco, USA) and 1% penicillin/streptomycin (Gibco, USA) in a humidified atmosphere of 5% CO_2 at 37°C.

Tissue collection

Fifty NSCLC tissues and matched adjacent non-tumor tissues were obtained from the Affiliated Hospital of Qingdao University. These tissues were immediately frozen in liquid nitrogen and then stored at −80°C. The Institutional Review Board of the Affiliated Hospital of Qingdao University approved human tissue study and signed the informed consent with all patients before the research started. Table 1 shows the patients' clinical characteristics.

Pull-down assay with biotinylated circ0001666 probe

We fixed 1×10^7 NSCLC cells with 1% paraformaldehyde, harvested, lysed, sonicated, and centrifugated. The biotinylated circ0001666 probe and oligo probe (Tsingke, China) were incubated with M-280 streptavidin magnetic beads (Invitrogen, USA) at room temperature for 2 h to generate probe-coated beads. Then, 20 μL supernatant was harvested as input, and the remaining was incubated with probe-coated beads at 4°C overnight. The beads were washed thoroughly with wash buffer. Then, proteinase K was used to reverse the formaldehyde cross-linking. The RNA complexes bound to the beads were eluted and extracted with RNeasy Mini Kit (Qiagen) and analyzed by quantitative real-time PCR assays.

Pull-down assay with biotinylated miRNA

NSCLC cells were transfected with biotin-labeled miRNA mimics or control (Tsingke, China) for 48 h. Then, cells were harvested and sonicated. Fifty microliters of the lysates were used as input, and the remaining lysates were incubated with M-280 streptavidin magnetic beads (Invitrogen, USA) at 4°C on the rotator overnight. Next, the beads were washed strictly with wash buffer. The RNAs bound to magnetic beads were purified with RNeasy Mini kit (QIAGEN) and analyzed by quantitative real-time PCR. The information of biotinylated probes was provided in the Table S1.

Western blot analysis

Cells were lysed in radioimmunoprecipitation assay (RIPA) buffer (CWBIO, China) with protease and phosphatase inhibitors (CWBIO, China). An equal amount of total protein lysates (30 ng) was separated by 10% SDS-PAGE and transferred onto a polyvinylidene fluoride (PVDF) membrane and then incubated with primary antibodies specific for AGO1 (1:1,000 dilution; Proteintech, USA), anti-PI3Kinase p85 (1:1,000 dilution; Cell Signaling Technology, USA), phospho-PI3-Kinase p85 (1:1,000 dilution; Cell Signaling Technology, USA), anti-AKT kinase (1:1,000 dilution; Cell Signaling Technology, USA), phospho-AKT (Ser 473, 1:1,000 dilution; Cell Signaling Technology, USA), anti-mTOR (1:1,000 dilution; Cell Signaling Technology, USA), phospho-mTOR (1:1,000 dilution; Cell Signaling Technology, USA), and GAPDH (1:1,000 dilution; Proteintech, China) at 4°C overnight, followed by incubation with appropriate horseradish peroxidase (HRP)-conjugated secondary antibodies at room temperature for 2 h. Bands were visualized using Immobilon ECL substrate kit (Millipore, Germany), and the images were captured via Bio Spectrum 600 Imaging System (UVP, USA).

RNA extraction, RNase R treatment, and polymerase chain reaction (quantitative real-time PCR)

Total RNA was extracted from cells and tissues using Trizol reagent (Invitrogen) according to the manufacturer's protocols. circRNA and mRNA were reversely transcribed using the PrimeScript RT Master Mix (Takara, Japan). For RNase R treatment, 2 μg of total RNA extracted from NSCLC cells was incubated with or without 3 U/g RNase R (Epicenter, USA) at 37°C for 15 min. Quantitative real-time PCR was performed using SYBR Premix Ex Taq kit (Takara, Japan) for the detection of circRNAs and mRNA expression. GAPDH was used as internal references. The sequences of primers are provided in the Table S1. The $2^{-\triangle\triangle Ct}$ method was used to calculate relative expression of RNA.

Bioinformatics analysis

The sequence of circ0001666 was acquired from circBase (http://www.circbase.org). The miRNA-binding sites in AGO1 were acquired from TargetScan (http://www.targetscan.org) and miRDB (http://www.mirdb.org). CircInteractome (https://circinteractome.nia.nih.gov), Circbank (http://www.circbank.cn), and miRanda (http://www.microrna.org) were used to predict the miRNA-binding sites located in circ0001666.

Plasmid construction and cell transfection

Hsa_circ_0001666 was synthesized by Tsingke (China) company and cloned into pcDNA3.1(+) CircRNA Mini Vector (Geenseed Biotech, China), and AGO1 cDNA was amplified by PCR and cloned into pcDNA3.1(+) vector (Invitrogen, USA). Oligos of circ0001666 and AGO1 short hairpin RNAs (shRNAs) were synthesized and inserted into GV298/Cherry/Puro vector (BioVector, China). The miRNA mimics were transfected into NSCLC cells using RNAiMAX (Invitrogen, USA) according to the manufacturer's instructions. Lipofectamine 3000 (Life Technologies, USA) was used to deliver the plasmids into NSCLC cells according to the manufacturer's instructions. The circ0001666 overexpression plasmid was transfected into A549 and H1299 cells, and the cells were selected with G418 (Life Technologies, USA) for 4 weeks to establish stable cell lines. shRNA vectors were transfected into A549 and H1299 cell lines, and the transfected cells were stably selected with 1 μg/mL of puromycin (Gibco, USA) for 1 month.

Wound healing, migration, and invasion assays

For wound healing assays, a 200-μL pipette tip was used to create scratch wound in six-well plates when cells grew to 90%

AGO1-3′ UTR-mut and the miR-1184/miR-548I mimics or miR-1184/miR-548I inhibitors. (D) The protein levels of AGO1 in treated A549 and H1299 cells were evaluated through western blotting assays. (E and F) The expression levels of AGO1 were determined by quantitative real-time PCR (E) and western blot (F) in cell transfected with miR-1184/miR-548I mimics alone or co-transfected with circ0001666. *$p < 0.05$, ***$p < 0.001$.

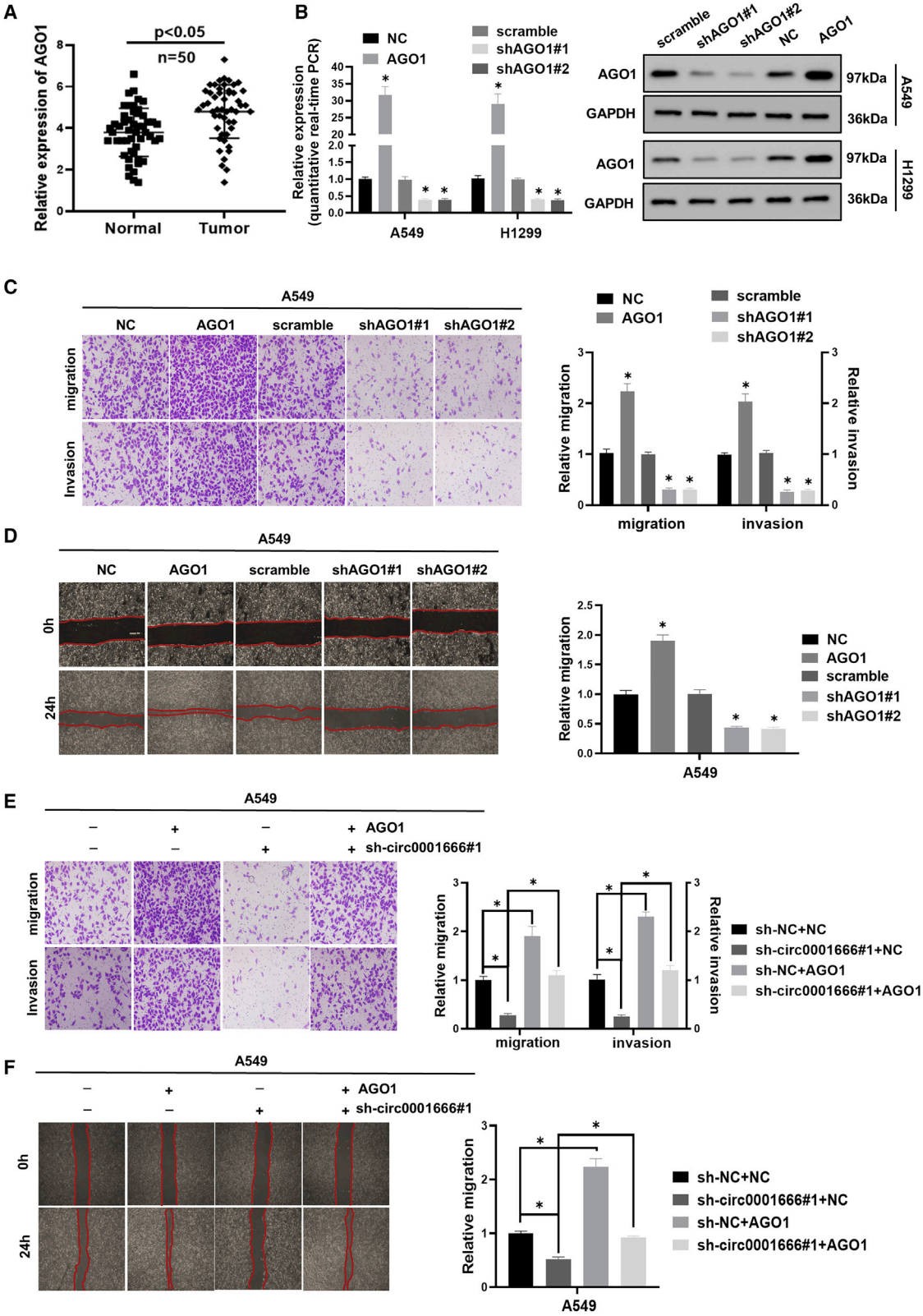

(legend on next page)

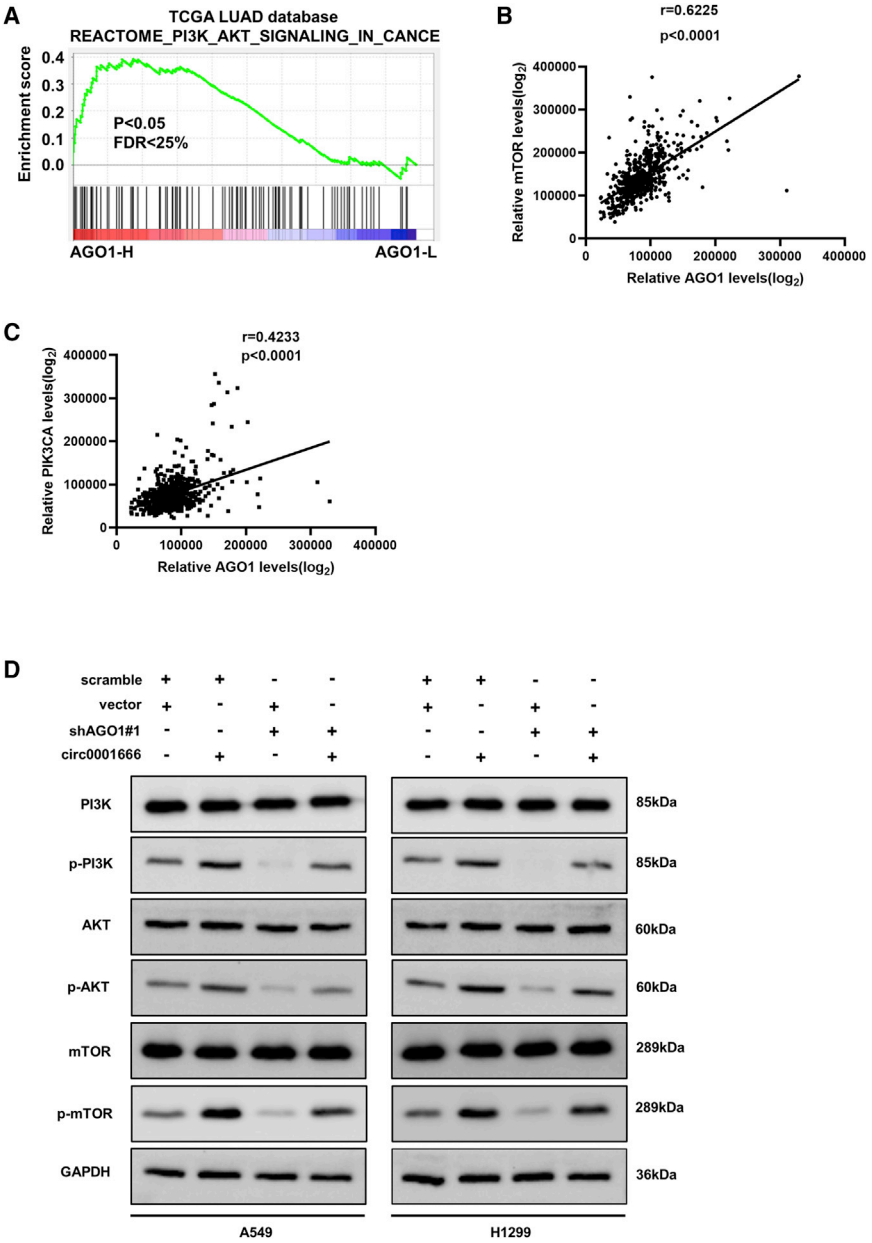

Figure 7. circ0001666 activates the PI3K/AKT/mTOR signaling pathways by regulating the expression of AGO1

(A–C) GSEA plot showed the correlation between AGO1 and PI3K/AKT/mTOR signaling pathway. (D) Western blot analysis showed the protein levels of PI3K, p-PI3K, AKT, p-AKT, mTOR, and p-mTOR in NSCLC cells transfected with circ0001666 or sh-AGO1 or the corresponding negative control. *p < 0.05.

confluence, and then the cells were cultured with serum-free medium immediately and were incubated for 24 h. Cell migration was photographed, and the distance was measured and normalized to the 0-h control as the relative migration rate for comparison.

For transwell migration and invasion assays, chambers with Matrigel (BD Biosciences, USA) were used for cell invasion assays, and chambers without Matrigel were used for cell migration assays according to the manufacturer's protocol. Cells suspended in 200 μL serum-free medium (5×10^4 cells/well for migration, 1×10^5 cells/well for invasion) were added to the upper chambers. F-12 or DMEM containing 20% fetal bovine serum (FBS) was added to the lower chambers. After incubation at 37°C for 24 h (migration assay) or 48 h (invasion assay), cells on the upper surface were removed with a cotton swab. Then, cells on the lower surface were fixed with methanol and stained with 0.1% crystal violet for photographing and counting.

Dual-luciferase reporter assay

A549 and H1299 cells were seeded in 24-well plate (6×10^4 cells per well) for 24 h before transfection. After transient transfection with constructed luciferase plasmids and miRNA mimics for 48 h, Rluc activity was measured with a dual-luciferase reporter assay system (Promega, USA) according to the manufacturer's protocols.

RNA immunoprecipitation (RIP) assay

RIP assays were determined using the Magna RIP kit (Millipore, Billerica, MA, USA) according to the manufacturer's instructions. The treated cell lysates were incubated with immunoprecipitation buffer containing anti-AGO2-conjugated magnetic beads or negative control anti-IgG at 4°C for

Figure 6. AGO1 is upregulated in NSCLC cells and promotes NSCLC cell migration and invasion

(A) The expression levels of AGO1 in 50 pairs of NSCLC and corresponding adjacent tissues were measured by quantitative real-time PCR. (B) The efficiency of AGO1 knockdown and overexpression was analyzed by quantitative real-time PCR and western blot analysis. (C) Representative images and quantification results of transwell assays for A549 cells transfected with AGO1 or shAGO1 are shown. (D) Representative images and quantification results of wound healing assays for A549 cells transfected with AGO1 or shAGO1 are shown. (E) Representative images and quantification results of A549 cells after transfecting with AGO1 alone or co-transfected with sh-circ0001666 are shown. (F) Representative images and quantification results of wound healing assays for A549 cells after transfecting with AGO1 alone or co-transfected with sh-circ0001666 are shown. *p < 0.05.

24 h. Then, the immunoprecipitated RNA was extracted and purified. The enrichment of the target RNA was evaluated by quantitative real-time PCR.

FISH

The Cy3-labeled circ0001666 probe and Dig-labeled miR-1184/miR-548I probes were constructed by RiboBio (Guangzhou, China). The signals of the probes were detected by the Fluorescent *In Situ* Hybridization Kit (RiboBio, China) according to the manufacturer's instructions. All fluorescent images were captured using Nikon A1Si Laser Scanning Confocal Microscope (Nikon Instruments, Japan).

Animal studies

The animal studies were carried out in accordance with NIH Guidelines for the Care and Use of Laboratory Animals and approved by the Animal Care Committee of Tongji Medical College. Four-week-old male BALB/c nude mice were randomly divided into three groups (n = 5 per group). We injected 2×10^6 cells into each mouse caudal vein to establish the lung metastasis model. Two months later, all mice were anesthetized with 10 mg/kg toluene thiazide and euthanized with cervical dislocation. Subsequently, the lungs were resected and pathological examination was performed. We used an In Vivo optical imaging system (IN VIVO FX Pro, Bruker, USA) to obtain fluorescent images of xenografts in nude mice. The lungs were paraffin embedded, and the metastasis was confirmed with hematoxylin and eosin (H&E) staining.

Statistical analysis

Data were presented as the mean ± standard error of the mean (SEM). Statistical analyses were conducted using GraphPad Prism 8.0 software (La Jolla, USA). Statistical differences between the two groups were assessed using the t test (two-tailed). $p < 0.05$ was considered statistically significant.

SUPPLEMENTAL INFORMATION

Supplemental information can be found online at https://doi.org/10.1016/j.omto.2022.02.011.

ACKNOWLEDGMENTS

The present study was supported by Chinese Society of Clinical Oncology Research Foundation, China (grant nos. Y-HS2019-27 and Y-QL202101-0258).

AUTHOR CONTRIBUTIONS

Z.Y. and W.W. conceived and designed the experiments. X.W. and L.F. performed most of the experiments and data analysis. X.W. and R.L. drafted the manuscript. J.W., Q.Q., and X.W. performed the bioinformatic analysis and revised the work critically for important intellectual content. W.W. and X.W. helped with the *in vivo* experiments. X.W., Q.Q., and L.F. collected the clinical samples and information. All authors read and approved the final manuscript.

DECLARATION OF INTERESTS

The authors declare no competing interests.

REFERENCES

1. Siegel, R.L., Miller, K.D., Fuchs, H.E., and Jemal, A. (2021). Cancer statistics, 2021. CA: a Cancer J. clinicians *71*, 7–33.
2. Herbst, R.S., Morgensztern, D., and Boshoff, C. (2018). The biology and management of non-small cell lung cancer. Nature *553*, 446–454.
3. Saab, S., Zalzale, H., Rahal, Z., Khalifeh, Y., Sinjab, A., and Kadara, H. (2020). Insights into lung cancer immune-based biology, prevention, and treatment. Front. Immunol. *11*, 159.
4. Suresh, K., Naidoo, J., Lin, C.T., and Danoff, S. (2018). Immune checkpoint immunotherapy for non-small cell lung cancer: benefits and pulmonary Toxicities. Chest *154*, 1416–1423.
5. Duma, N., Santana-Davila, R., and Molina, J.R. (2019). Non-small cell lung cancer: epidemiology, screening, diagnosis, and treatment. Mayo Clinic Proc. *94*, 1623–1640.
6. Chen, R., Manochakian, R., James, L., Azzouqa, A.G., Shi, H., Zhang, Y., Zhao, Y., Zhou, K., and Lou, Y. (2020). Emerging therapeutic agents for advanced non-small cell lung cancer. J. Hematol. Oncol. *13*, 58.
7. Zhu, T., Bao, X., Chen, M., Lin, R., Zhuyan, J., Zhen, T., Xing, K., Zhou, W., and Zhu, S. (2020). Mechanisms and future of non-small cell lung cancer metastasis. Front. Oncol. *10*, 585284.
8. Wu, S.G., and Shih, J.Y. (2018). Management of acquired resistance to EGFR TKI-targeted therapy in advanced non-small cell lung cancer. Mol. Cancer *17*, 38.
9. Assi, H.I., Kamphorst, A.O., Moukalled, N.M., and Ramalingam, S.S. (2018). Immune checkpoint inhibitors in advanced non-small cell lung cancer. Cancer *124*, 248–261.
10. de Sousa, V.M.L., and Carvalho, L. (2018). Heterogeneity in lung cancer. Pathobiology: J. immunopathology, Mol. Cell. Biol. *85*, 96–107.
11. Jeck, W.R., and Sharpless, N.E. (2014). Detecting and characterizing circular RNAs. Nat. Biotechnol. *32*, 453–461.
12. Memczak, S., Jens, M., Elefsinioti, A., Torti, F., Krueger, J., Rybak, A., Maier, L., Mackowiak, S.D., Gregersen, L.H., Munschauer, M., et al. (2013). Circular RNAs are a large class of animal RNAs with regulatory potency. Nature *495*, 333–338.
13. Lei, B., Tian, Z., Fan, W., and Ni, B. (2019). Circular RNA: a novel biomarker and therapeutic target for human cancers. Int. J. Med. Sci. *16*, 292–301.
14. Li, Z., Ruan, Y., Zhang, H., Shen, Y., Li, T., and Xiao, B. (2019). Tumor-suppressive circular RNAs: mechanisms underlying their suppression of tumor occurrence and use as therapeutic targets. Cancer Sci. *110*, 3630–3638.
15. Zhang, H.D., Jiang, L.H., Sun, D.W., Hou, J.C., and Ji, Z.L. (2018). CircRNA: a novel type of biomarker for cancer. Breast Cancer (Tokyo, Japan) *25*, 1–7.
16. Arnaiz, E., Sole, C., Manterola, L., Iparraguirre, L., Otaegui, D., and Lawrie, C.H. (2019). CircRNAs and cancer: biomarkers and master regulators. Semin. Cancer Biol. *58*, 90–99.
17. Wang, S., Zhang, K., Tan, S., Xin, J., Yuan, Q., Xu, H., Xu, X., Liang, Q., Christiani, D.C., Wang, M., et al. (2021). Circular RNAs in body fluids as cancer biomarkers: the new frontier of liquid biopsies. Mol. Cancer *20*, 13.
18. Kristensen, L.S., Andersen, M.S., Stagsted, L.V.W., Ebbesen, K.K., Hansen, T.B., and Kjems, J. (2019). The biogenesis, biology and characterization of circular RNAs. Nat. Rev. Genet. *20*, 675–691.
19. Li, B., Zhu, L., Lu, C., Wang, C., Wang, H., Jin, H., Ma, X., Cheng, Z., Yu, C., Wang, S., et al. (2021). circNDUFB2 inhibits non-small cell lung cancer progression via destabilizing IGF2BPs and activating anti-tumor immunity. Nat. Commun. *12*, 295.
20. Zhang, P.F., Pei, X., Li, K.S., Jin, L.N., Wang, F., Wu, J., and Zhang, X.M. (2019). Circular RNA circFGFR1 promotes progression and anti-PD-1 resistance by sponging miR-381-3p in non-small cell lung cancer cells. Mol. Cancer *18*, 179.
21. Wang, L., Tong, X., Zhou, Z., Wang, S., Lei, Z., Zhang, T., Liu, Z., Zeng, Y., Li, C., Zhao, J., et al. (2018). Circular RNA hsa_circ_0008305 (circPTK2) inhibits TGF-β-induced epithelial-mesenchymal transition and metastasis by controlling TIF1γ in non-small cell lung cancer. Mol. Cancer *17*, 140.
22. Zhang, R., Zhu, W., Ma, C., and Ai, K. (2021). Silencing of circRNA circ_0001666 represses EMT in pancreatic cancer through upregulating miR-1251 and downregulating SOX4. Front. Mol. biosciences *8*, 684866.
23. Qi, Y., He, J., Zhang, Y., Wang, L., Yu, Y., Yao, B., and Tian, Z. (2021). Circular RNA hsa_circ_0001666 sponges miR-330-5p, miR-193a-5p and miR-326, and promotes

papillary thyroid carcinoma progression via upregulation of ETV4. Oncol. Rep. *45*, 50.

24. Ashrafizadeh, M., Zarrabi, A., Hushmandi, K., Hashemi, F., Moghadam, E.R., Owrang, M., Hashemi, F., Makvandi, P., Goharrizi, M., Najafi, M., et al. (2021). Lung cancer cells and their sensitivity/resistance to cisplatin chemotherapy: role of microRNAs and upstream mediators. Cell Signal. *78*, 109871.
25. Mirzaei, S., Zarrabi, A., Hashemi, F., Zabolian, A., Saleki, H., Ranjbar, A., Seyed Saleh, S.H., Bagherian, M., Sharifzadeh, S.O., Hushmandi, K., et al. (2021). Regulation of Nuclear Factor-KappaB (NF-κB) signaling pathway by non-coding RNAs in cancer: inhibiting or promoting carcinogenesis? Cancer Lett. *509*, 63–80.
26. Paskeh, M.D.A., Mirzaei, S., Orouei, S., Zabolian, A., Saleki, H., Azami, N., Hushmandi, K., Baradaran, B., Hashmi, M., Aref, A.R., et al. (2021). Revealing the role of miRNA-489 as a new onco-suppressor factor in different cancers based on pre-clinical and clinical evidence. Int. J. Biol. macromolecules *191*, 727–737.
27. Ashrafizadeh, M., Zarrabi, A., Orouei, S., Zabolian, A., Saleki, H., Azami, N., Bejandi, A.K., Mirzaei, S., Janaghard, M.N., Hushmandi, K., et al. (2021). Interplay between SOX9 transcription factor and microRNAs in cancer. Int. J. Biol. macromolecules *183*, 681–694.
28. Mirzaei, S., Zarrabi, A., Asnaf, S.E., Hashemi, F., Zabolian, A., Hushmandi, K., Raei, M., Goharrizi, M., Makvandi, P., Samarghandian, S., et al. (2021). The role of microRNA-338-3p in cancer: growth, invasion, chemoresistance, and mediators. Life Sci. *268*, 119005.
29. Hansen, T.B., Jensen, T.I., Clausen, B.H., Bramsen, J.B., Finsen, B., Damgaard, C.K., and Kjems, J. (2013). Natural RNA circles function as efficient microRNA sponges. Nature *495*, 384–388.
30. Wu, P., Mo, Y., Peng, M., Tang, T., Zhong, Y., Deng, X., Xiong, F., Guo, C., Wu, X., Li, Y., et al. (2020). Emerging role of tumor-related functional peptides encoded by lncRNA and circRNA. Mol. Cancer *19*, 22.
31. Meng, S., Zhou, H., Feng, Z., Xu, Z., Tang, Y., Li, P., and Wu, M. (2017). CircRNA: functions and properties of a novel potential biomarker for cancer. Mol. Cancer *16*, 94.
32. Heavey, S., O'Byrne, K.J., and Gately, K. (2014). Strategies for co-targeting the PI3K/AKT/mTOR pathway in NSCLC. Cancer Treat. Rev. *40*, 445–456.
33. Wang, C., Tan, S., Li, J., Liu, W.R., Peng, Y., and Li, W. (2020). CircRNAs in lung cancer - biogenesis, function and clinical implication. Cancer Lett. *492*, 106–115.
34. Li, X., Yang, L., and Chen, L.L. (2018). The biogenesis, functions, and challenges of circular RNAs. Mol. cell *71*, 428–442.
35. Patop, I.L., Wüst, S., and Kadener, S. (2019). Past, present, and future of circRNAs. EMBO J. *38*, e100836.
36. Lasda, E., and Parker, R. (2014). Circular RNAs: diversity of form and function. RNA *20*, 1829–1842.
37. Dong, W., Bi, J., Liu, H., Yan, D., He, Q., Zhou, Q., Wang, Q., Xie, R., Su, Y., Yang, M., et al. (2019). Circular RNA ACVR2A suppresses bladder cancer cells proliferation and metastasis through miR-626/EYA4 axis. Mol. Cancer *18*, 95.
38. Ding, L., Zhao, Y., Dang, S., Wang, Y., Li, X., Yu, X., Li, Z., Wei, J., Liu, M., and Li, G. (2019). Circular RNA circ-DONSON facilitates gastric cancer growth and invasion via NURF complex dependent activation of transcription factor SOX4. Mol. Cancer *18*, 45.
39. Liu, Z., Wang, Q., Wang, X., Xu, Z., Wei, X., and Li, J. (2020). Circular RNA cIARS regulates ferroptosis in HCC cells through interacting with RNA binding protein ALKBH5. Cell Death Discov. *6*, 72.
40. He, Q., Zhao, L., Liu, X., Zheng, J., Liu, Y., Liu, L., Ma, J., Cai, H., Li, Z., and Xue, Y. (2019). MOV10 binding circ-DICER1 regulates the angiogenesis of glioma via miR-103a-3p/miR-382-5p mediated ZIC4 expression change. J. Exp. Clin. Cancer Res. CR *38*, 9.
41. Wang, L., Liang, Y., Mao, Q., Xia, W., Chen, B., Shen, H., Xu, L., Jiang, F., and Dong, G. (2019). Circular RNA circCRIM1 inhibits invasion and metastasis in lung adenocarcinoma through the microRNA (miR)-182/miR-93-leukemia inhibitory factor receptor pathway. Cancer Sci. *110*, 2960–2972.
42. Chen, L., Yang, X., Zhao, J., Xiong, M., Almaraihah, R., Chen, Z., and Hou, T. (2020). Circ_0008532 promotes bladder cancer progression by regulation of the miR-155-5p/miR-330-5p/MTGR1 axis. J. Exp. Clin. Cancer Res. CR *39*, 94.
43. Jiang, P., Zhu, Y., Xu, Z., Chen, X., and Xie, L. (2020). Interference with circBC048201 inhibits the proliferation, migration, and invasion of bladder cancer cells through the miR-1184/ITGA3 axis. Mol. Cell. Biochem. *474*, 83–94.
44. Wang, X., Chen, Y., Liu, W., Liu, T., and Sun, D. (2020). Hsa_circ_0128846 promotes tumorigenesis of colorectal cancer by sponging hsa-miR-1184 and releasing AJUBA and inactivating Hippo/YAP signalling. J. Cell. Mol. Med. *24*, 9908–9924.
45. Jia, C., Yao, Z., Lin, Z., Zhao, L., Cai, X., Chen, S., Deng, M., and Zhang, Q. (2021). circNFATC3 sponges miR-548I acts as a ceRNA to protect NFATC3 itself and suppressed hepatocellular carcinoma progression. J. Cell. Physiol. *236*, 1252–1269.
46. Faehnle, C.R., and Joshua-Tor, L. (2007). Argonautes confront new small RNAs. Curr. Opin. Chem. Biol. *11*, 569–577.
47. Wu, G., Fan, F., Hu, P., and Wang, C. (2020). AGO1 enhances the proliferation and invasion of cholangiocarcinoma via the EMT-associated TGF-β signaling pathway. Am. J. translational Res. *12*, 2890–2902.
48. Wang, M., Zhang, L., Liu, Z., Zhou, J., Pan, Q., Fan, J., Zang, R., and Wang, L. (2018). AGO1 may influence the prognosis of hepatocellular carcinoma through TGF-β pathway. Cell Death Dis. *9*, 324.
49. Kim, J.S., Choi, Y.Y., Jin, G., Kang, H.G., Choi, J.E., Jeon, H.S., Lee, W.K., Kim, D.S., Kim, C.H., Kim, Y.J., et al. (2010). Association of a common AGO1 variant with lung cancer risk: a two-stage case-control study. Mol. carcinogenesis *49*, 913–921.

OMTO, Volume *24*

Supplemental information

Hsa_circ_0001666 promotes non-small cell lung cancer migration and invasion through miR-1184/miR-548l/AGO1 axis

Xueting Wang, Rui Li, Lingxin Feng, Jing Wang, Qi Qi, Wenjie Wei, and Zhuang Yu

Fig.S1

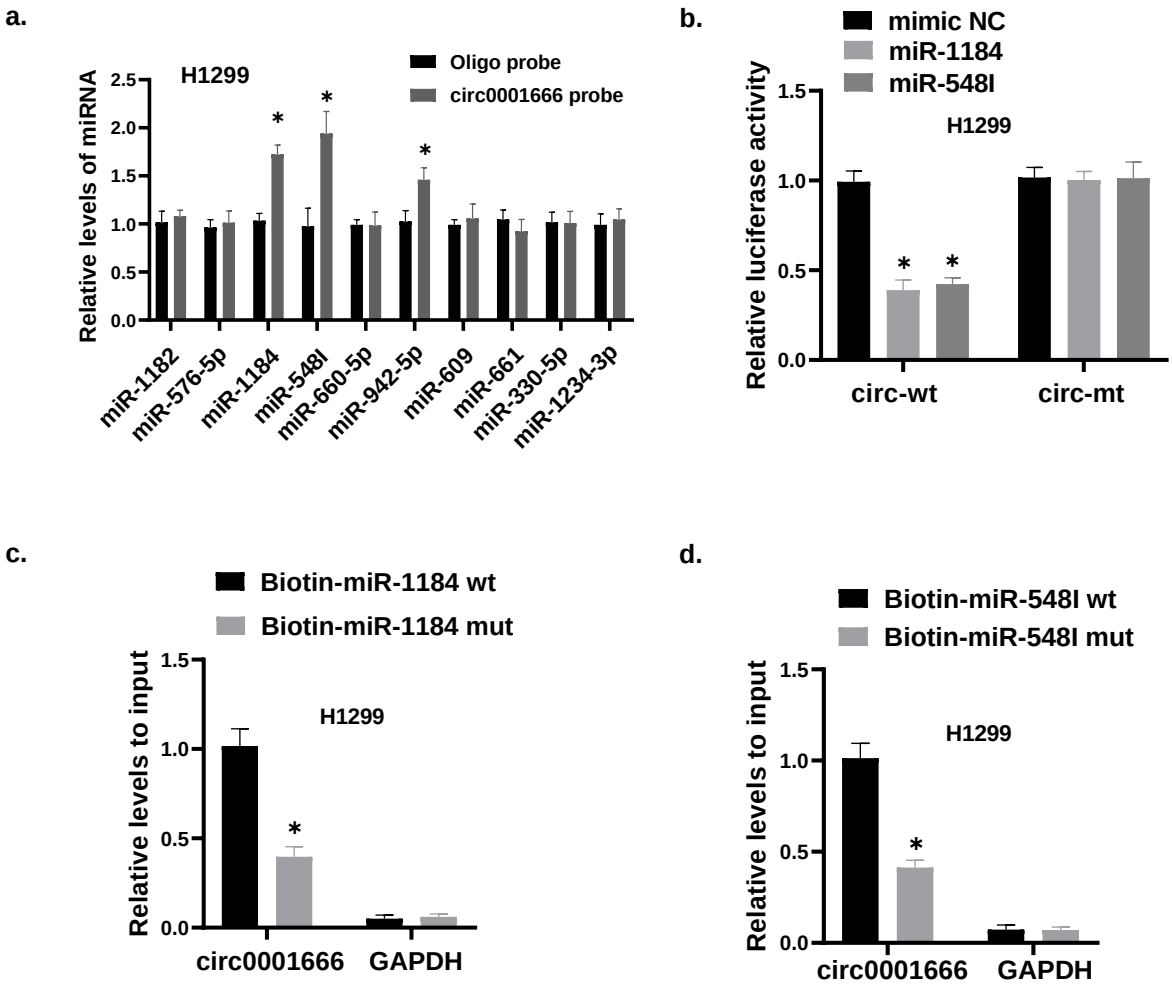

Fig.S1 Circ0001666 could bind to miR-1184 and miR-548I in H1299 cells.

a The relative levels of 10 candidate miRNAs were pulled down by circ0001666 probe or oligo probe in H1299 cells. **b** The luciferase activity after co-transfection with circ0001666-wt or circ0001666-mut and miR-1184/miR-548I mimics or vector in H1299 cells. **c-d** Relative levels of circ0001666 were captured by biotinylated wild-type miR-1184/miR-548I or mutant miR-1184/miR-548I in H1299 cells.

Fig.S2

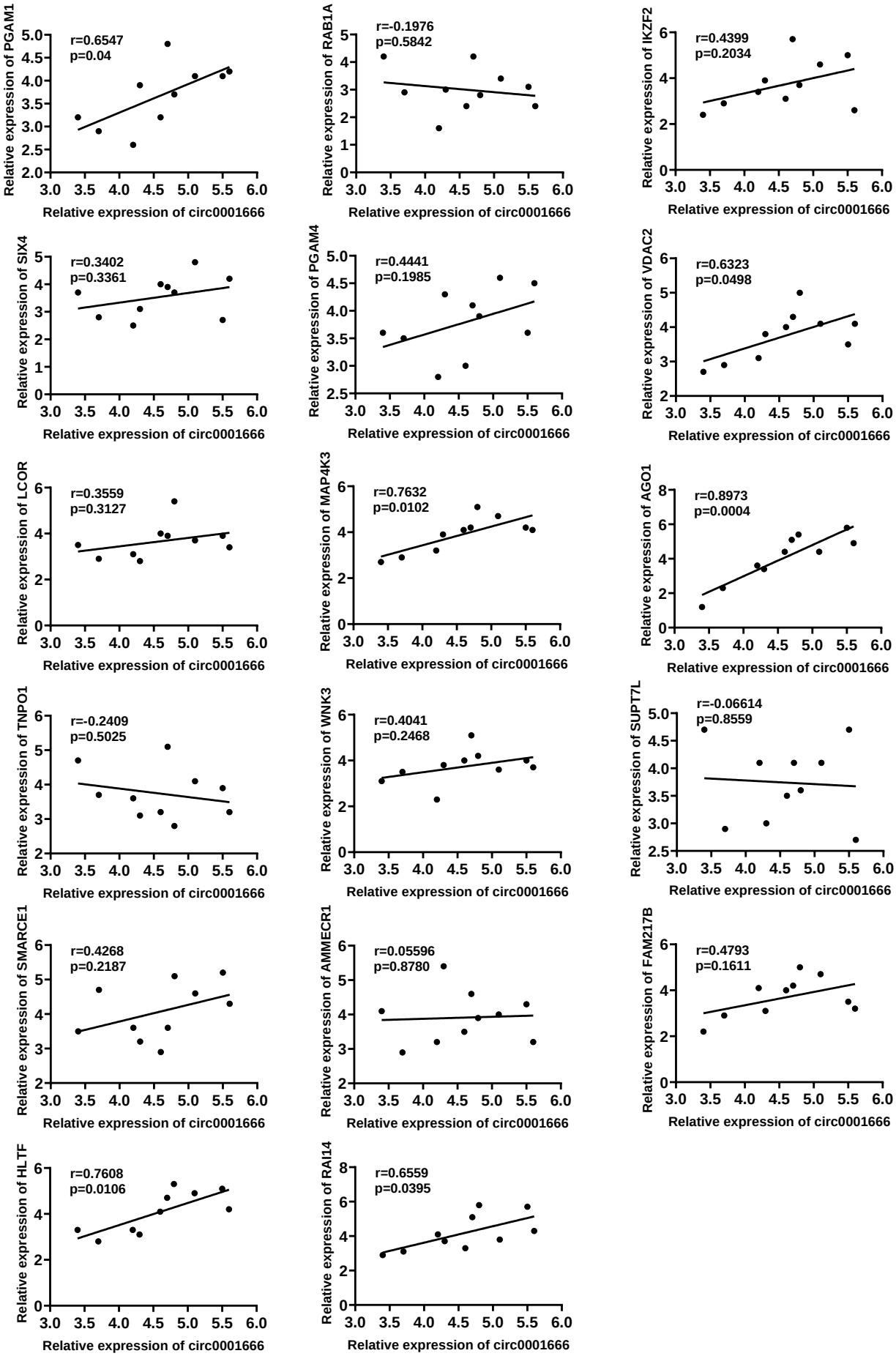

Fig.S2 The correlation between circ0001666 and 17 candidate targets genes mRNA in our NSCLC samples.

Supplementary Tables

Supplementary table 1 The sequences of primers, oligonucleotides and probes used in this study. Primers for PCR（5’-3'）

Divergent-circ0001666 F	GCCTAGCTGTCAAGGAGTGGTT
Divergent-circ0001666 R	GCCACCGCAGATCCAAGATT
Convergent-circ0001666 F	AGCACCACCGAAGCAAGTATCC
Convergent-circ0001666 R	TCTTATCCTGCTCCACCATGCC
linear-FAM120B F	CATGAGCAGTGGAGAGATTGA
linear-FAM120B R	GTGCTGGTGACATCTTGACAG
GAPDH F	AAATCAAGTGGGGCGATGCTG
GAPDH R	GCAGGAGGCATTGCTGATGAT
Divergent-GAPDH F	GAAGGTGAAGGTCGAGTC
Divergent-GAPDH R	GAAGATGGTGATGGGATTTC
hsa-miR-1182 F	GGAGGGTCTTGGGAGGGA
hsa-miR-1182 R	AGTGCAGGGTCCGAGGTATT
hsa-miR-567-5p F	GCGCGATTCTAATTTCTCCAC
hsa-miR-567-5p R	AGTGCAGGGTCCGAGGTATT
hsa-miR-1184 F	CGCCTGCAGCGACTTGATG
hsa-miR-1184 R	AGTGCAGGGTCCGAGGTATT
hsa-miR-548I F	GCGAAAAGTATTTGCGGGT
hsa-miR-548I R	AGTGCAGGGTCCGAGGTATT
hsa-miR-660-5p F	CGCGTACCCATTGCATATCG
hsa-miR-660-5p R	AGTGCAGGGTCCGAGGTATT
hsa-miR-942-5p F	CGCGTCTTCTCTGTTTTGGC
hsa-miR-942-5p R	AGTGCAGGGTCCGAGGTATT
hsa-miR-609 F	GCGCGAGGGTGTTTCTCTC
hsa-miR-609 R	AGTGCAGGGTCCGAGGTATT
hsa-miR-661 F	TGCCTGGGTCTCTGGCCT
hsa-miR-661 R	AGTGCAGGGTCCGAGGTATT
hsa-miR-330-5p F	GCGTCTCTGGGCCTGTGTC
hsa-miR-330-5p R	AGTGCAGGGTCCGAGGTATT
hsa-miR-1234-3p F	TCGGCCTGACCACCCA
hsa-miR-1234-3p R	AGTGCAGGGTCCGAGGTATT
PGAM1 F	GGCACAGGTATTTGGCCTCA
PGAM1 R	CAAACTCATAGCCAGCATCAGAC
RAB1A F	TGCCTTCTTCTTAGGTTTGCA
RAB1A R	GGCCTGCTGTGTCCCATATTT
IKZF2 F	TGTGGACGAAGCTACAAGCA
IKZF2 R	CTTCCATAGGAGGTACATGGTGA
SIX4 F	TGGCAGCTTCACAAGGTAAT

SIX4 R	GGCCTGTATTAGGAACCGTG
PGAM4 F	AAGCCACGACCAATGAGGA
PGAM4 R	CACTGGAATGACTAGAGCCC
VDAC2 F	TCAGGACACCACCAGATTCC
VDAC2 R	TAATGACCTTGCGCTCTCACA
LCOR F	AGAACTGGATTCGTGGCG
LCOR R	AGGTCCAAACAGCCCTTCA
MAP4K3 F	AGTCTTTCATTGGCACACCA
MAP4K3 R	ACATAGGAGGCTGAAGCTCTG
AGO1 F	GAAACCAATCAAGCTCCTGGC
AGO1 R	TATTCCACCACTTCCCGGTTG
TNPO1 F	GGTGACTCCTCTCCTCTGATT
TNPO1 R	CACCAAATGCTCCCTCACAG
WNK3 F	GGCATAGTTGCTACAGATCCAC
WNK3 R	CCTTTGTCCAGTCATCCACCA
SUPT7L F	GTACCTCCTTGTCTCGGTTCA
SUPT7L R	TGTGAGATCCTTGCCTTTACC
SMARCE1 F	CACCAGGGTTTGTGGGATACA
SMARCE1 R	TGATACCAGAGGATGCCGTGA
AMMECR1 F	CAACGAGCCCTATGCCCTTA
AMMECR1 R	ACCCACCTCCCAGTCCAAATA
FAM217B F	AGTGCTCTGGCTATTGCTGAA
FAM217B R	TCTCCTCACCACCGGAACTTT
HLTF F	AGCATAAGGTGGCTAAGAGTGA
HLTF R	CTGGATTGGAGTACCTGTCAA
RAI14 F	GAGGAAGGAGAGGAAGGTGTTG
RAI14 R	AGTAGCCGGTCATCATTCTTGT
FISH probes	
circ0001666 (cy3)	Ribobio
U6 (cy3)	Ribobio
18s (cy3)	Ribobio
miR-1184 mimic (Dig)	Ribobio
miR-548I mimic (Dig)	Ribobio
Biotinylated probes	
circ0001666 probe	GAACTCCGGGAAAGGATCTGGAATGGTCATCTGC
(biotin) miR-1184 mimics	CCUUCGGUAGUUCAGCGACGUCC
(biotin) miR-1184 mutant	CCUUCGGUAGUUCAGCCUUUCGC
(biotin) miR-548I mimics	CUGUUUUGGGCGUUUAUGAAAA
(biotin) miR-548I mutant	CUGUUUUGGGCGUCACGCUUUC
lentivirus-shRNA	
GV298-NC-shRNA	BioVector

GV298-circ0001666-shRNA#1	GATGACCATTCCAGATCCTTTCTCGAGAAAGGATCTGGAATGGTCATC
GV298-circ0001666-shRNA#2	AGATGACCATTCCAGATCCTTCTCGAGAAGGATCTGGAATGGTCATCT
GV298-AGO1-shRNA#1	GGTGGAATACATCTCGAGATGTATTCCACCACTTCCC
GV298-AGO1-shRNA#2	GCTCCTGGCCAATTACTTTGACTCGAGTCAAAGTAATTGGCCAGGAGC